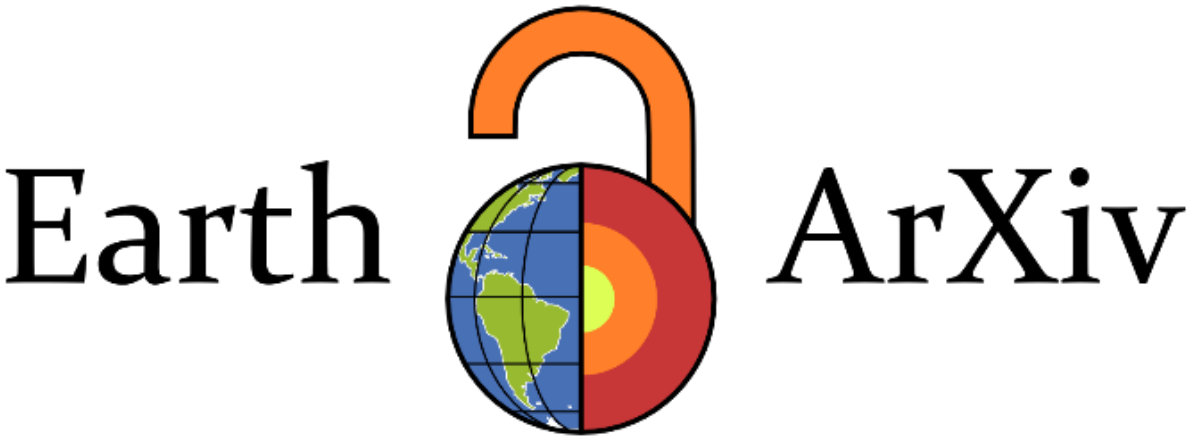

Joint Rock Physics Inversion and Basin Modeling for Comprehensive Source Rock Characterization

Jiayuan Huang, Department of Energy Science & Engineering, Stanford University, Stanford, California, USA. Email: jiayuanh@stanford.edu; ORCID: 0009-0008-6367-4711.

Tapan Mukerji, Department of Energy Science & Engineering, Stanford University, Stanford, California, USA; Department of Earth & Planetary Sciences, Stanford University, Stanford, California, USA; Department of Geophysics, Stanford University, Stanford, California, USA. E-mail: mukerji@stanford.edu.

Corresponding author: Jiayuan Huang, jiayuanh@stanford.edu

Keywords: Rock physics inversion; Basin modeling; Thermal maturity; Source rock characterization; Uncertainty quantification

ABSTRACT

This study presents an integrated workflow that combines statistical rock physics inversion with Monte Carlo basin modeling to comprehensively quantify source rock properties and their uncertainties. First, well-log and seismically-derived elastic properties are used in a statistical rock physics inversion to estimate porosity, kerogen content, and mineral fractions. These posterior distributions capture key compositional variability but provide limited constraint on thermal maturity due to weak sensitivity of elastic properties to thermally controlled changes. To address this limitation, inversion-derived properties are propagated through forward burial and thermal history simulations using Monte Carlo basin modeling. Uncertain geological and kinetic inputs, including geothermal history, erosion, and kerogen kinetics, are sampled to generate probabilistic predictions of vitrinite reflectance, transformation ratio, temperature, and pore pressure.

Application to the Goldwyer III source rock in the Canning Basin demonstrates that the integrated workflow reduces uncertainty in thermal maturity while maintaining consistency with geochemical indicators and measured temperature. The results reveal spatial variability in source rock quality and maturity that is not evident from elastic properties alone. This work establishes a practical, uncertainty-aware framework that couples geological, geophysical, geochemical, and geomechanical processes, ultimately improving confidence in hydrocarbon generation assessment and supporting risk reduction in exploration, particularly in frontier or data-limited settings.

INTRODUCTION

Comprehensively understanding source rock properties such as porosity, total organic carbon (TOC), mineral composition, fluid saturation, thermal maturity, and transformation ratio is fundamental for evaluating hydrocarbon generation potential and exploration risk (Peters et al., 2017). These properties influence reservoir quality, pore pressure evolution, and the overall effectiveness of a petroleum system. Rock physics provides the quantitative link between petrophysical properties and elastic properties such as V_P, V_S, and density, enabling interpretation of well logs and seismic attributes in terms of lithology, porosity, and pore fluids (Avseth et al., 2010).

However, rock physics inversion is inherently nonlinear and non-unique, as multiple combinations of porosity, mineralogy, kerogen content, and maturity may yield similar elastic responses (Bosch et al., 2010). Stochastic approaches are therefore preferred for uncertainty quantification in reservoir and source rock characterization (Grana et al., 2022).

Elastic properties of organic-rich shales are primarily controlled by porosity, mineral composition, kerogen, and fluids (Li et al., 2015). Although thermal maturation modifies kerogen

composition and structure, the direct influence on bulk rock elastic moduli is generally modest. Observable elastic deviations in mature source rocks are instead predominantly associated with fluid changes linked to hydrocarbon generation, as indicated by correlations with high resistivity and fluid-substitution predictions (Hansen et al., 2019). As a result, changes in vitrinite reflectance often produce subtle or non-unique elastic signatures that limit the ability of rock physics inversion alone to reliably resolve thermal maturity. In contrast, basin and petroleum system modeling (BPSM) integrates geological, geochemical, and geophysical inputs to simulate burial, thermal, and fluid-flow histories, providing a physics-based framework for predicting thermal maturity, transformation ratio, and associated pressure and temperature evolution over geological time (Hantschel & Kauerauf, 2009). When combined with Monte Carlo sampling, BPSM propagates uncertainties in key geological inputs—such as heat flow, erosion magnitude, and reaction kinetics—to generate probabilistic estimates of subsurface properties such as porosity, pore-pressure, and source rock thermal evolution (Tong & Mukerji, 2017; Fonseca et al., 2023).

Statistical rock physics inversion and Monte Carlo basin modeling provide complementary strengths for source rock characterization. Elastic data provide strong constraints on composition-controlled properties such as porosity, kerogen content, and mineral composition, whereas burial and thermal history modeling is better suited for estimating thermally-controlled properties such as thermal maturity and transformation ratio. These complementary roles motivate an integrated workflow in which statistical rock physics inversion is used to obtain posterior distributions of key petrophysical properties, which are then propagated as probabilistic inputs into a Monte Carlo basin modeling framework. In the basin modeling stage, uncertainties in heat flow, erosion magnitude, organic facies, and kinetic parameters are explicitly sampled to generate probabilistic

predictions of source rock thermal evolution and associated pressure–temperature histories. Figure 1 summarizes the proposed integrated workflow.

We apply the workflow to the Goldwyer III source rock in the Canning Basin, Western Australia, using well-log, geochemical, and seismically-derived elastic properties. The results demonstrate that combining statistical rock physics inversion with Monte Carlo basin modeling enables a more complete and uncertainty-aware characterization of source rock systems than either approach alone.

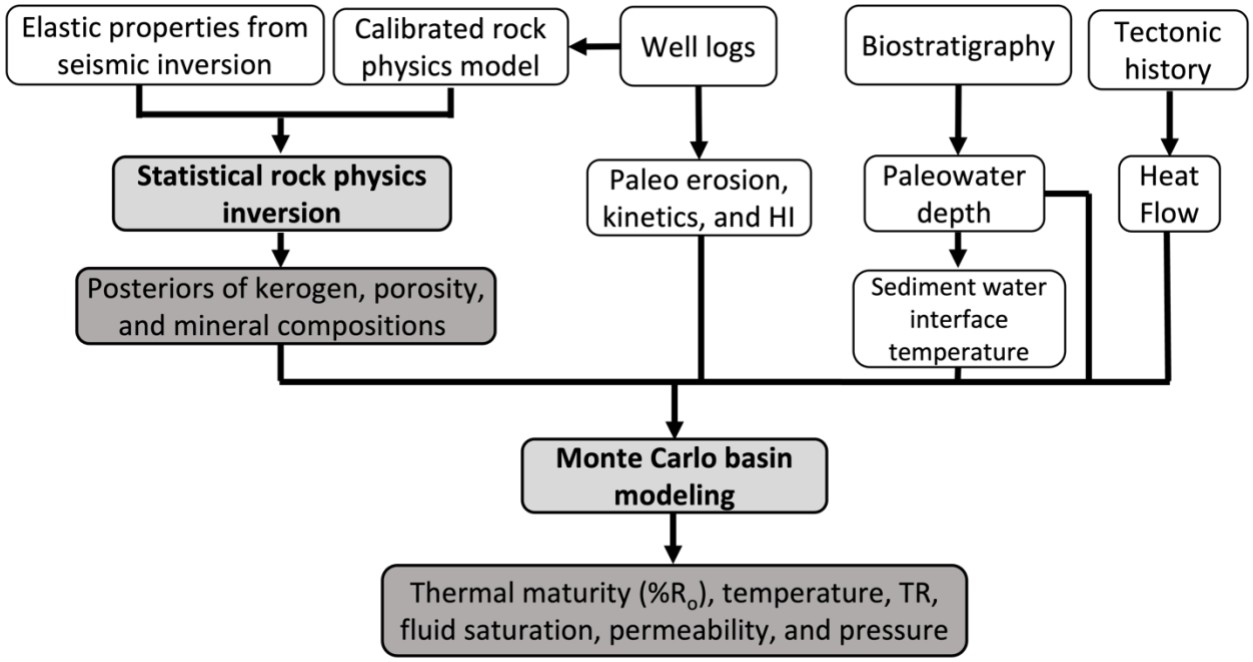

Figure 1. Integrated workflow combining statistical rock physics inversion and Monte Carlo basin modeling for source rock characterization. Posterior petrophysical properties from the inversion (porosity, kerogen content, mineral compositions) provide probabilistic inputs to basin modeling, which also samples uncertainties in heat flow, erosion, kinetics, and paleoenvironmental conditions to predict thermal maturity (Ro%), transformation ratio (TR), temperature, fluid saturation, permeability, and pressure. HI is hydrogen index.

STUDY AREA AND DATA

This study focuses on the Goldwyer III unit within the Broome Platform of the Canning Basin in northwestern Australia. The Canning Basin is a large Paleozoic intracratonic basin containing thick successions of marine shales, carbonates, and evaporites (D'Ercole et al., 2003). The Lower–Middle Ordovician Goldwyer Formation comprises an upper shale unit (Goldwyer I), a middle carbonate unit (Goldwyer II), and a lower organic-rich shale unit (Goldwyer III) (Foster et al., 1986). Goldwyer III is the primary source rock in the region, characterized by high TOC and predominantly oil- and gas-prone Type II–III kerogen (Johnson et al., 2020; Iqbal et al., 2022).

Regional tectonic events, including Ordovician–Silurian extension, Devonian–Carboniferous compression, and Jurassic–Cretaceous extension, produced multiple unconformities and variable subsidence histories that significantly influenced the burial and thermal evolution of the Goldwyer III source rock (Ghori et al., 2007; Haines, 2011). These tectonically driven burial variations form the basis for reconstructing the basin's thermal history in the Monte Carlo modeling stage.

The Theia-1 well is located within the Goldwyer III depocenter (Figure 2). Available well logs include petrophysical, geochemical, and sonic measurements, which are used to construct the rock physics model and define key inputs for basin modeling. A pre-stack seismic inversion section from the Carribuddy survey ties directly to Theia-1 (Figure 2 and 3), providing seismically-derived V_P, V_S, and density for application of the statistical rock physics inversion workflow.

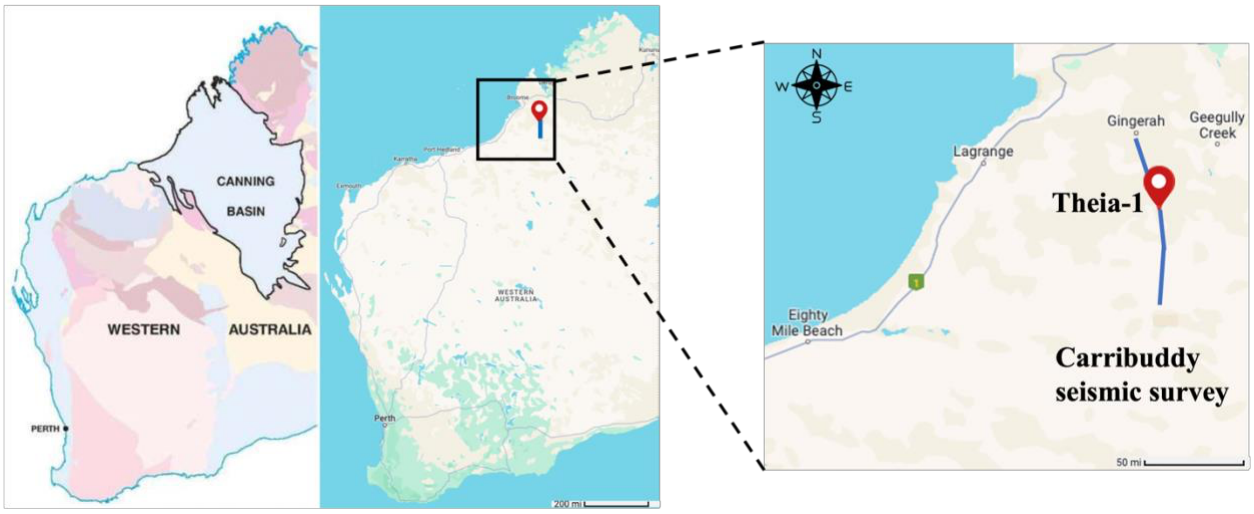

Figure 2. Locations of Theia-1 well and Carribuddy seismic survey in the Canning Basin. Red dot indicates the well location and the blue curve represents the 2-D seismic section.

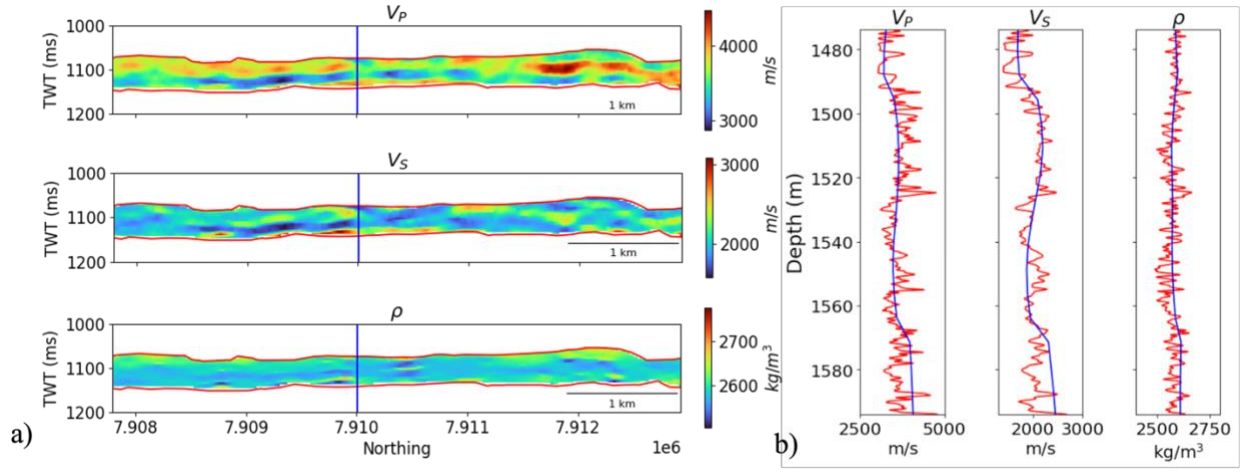

Figure 3. (a) Portion of the pre-stack seismic inversion section near the Theia-1 well. The blue vertical line marks the Theia-1 well, and the red horizons indicate the top and base of the Goldwyer III unit. (b) Comparisons of V_P, V_S, ρ between well logs (red) and seismic inversion results (blue) within the Goldwyer III interval at Theia-1.

STATISTICAL ROCK PHYSICS INVERSION

Rock physics inversion serves as the quantitative bridge between observed elastic properties and the underlying petrophysical characteristics. Here, we employ a rock physics model calibrated with well logs to generate forward predictions of elastic properties. A likelihood-free Bayesian inversion framework is then used to identify the petrophysical uncertainty consistent with wells and seismic data. Likelihood-free Bayesian methods such as Approximate Bayesian Computation (ABC) have gained attention for complex inverse problems where explicit likelihood formulations are impractical (Rubin, 1984; Pradhan & Mukerji, 2020; Pacchiardi et al., 2021). ABC enables probabilistic estimation of petrophysical properties by comparing simulated and observed elastic responses without requiring an explicit likelihood function, making it well suited for highly nonlinear rock physics models. The inversion provides spatially coherent, uncertainty-aware property estimates and their posterior distributions that can integrate directly with the basin modeling presented later.

Thermal-maturation dependent rock physics model. A thermal-maturity dependent rock physics model was used to simulate the elastic properties of organic-rich shale (Figure 4; Al Ibrahim et al., 2020). The inorganic mineral matrix and kerogen are modeled separately. Mineral matrix moduli are computed using standard Voigt–Reuss–Hill bounds, and pore fluids are represented as a single effective phase using the Reuss lower bound. Kerogen evolution is linked to vitrinite reflectance, which governs changes in organic porosity, hydrocarbon generation, and kerogen density through established empirical relationships (Sweeney & Burnham, 1990; Alfred & Vernik, 2012; Galford et al., 2013). Pores and fluid mixtures are incrementally added to the kerogen and inorganic matrix using the Differential Effective Medium (DEM) theory (Berryman,

1995). The resulting porous components are then upscaled with the Backus average (Backus, 1962) to obtain long-wavelength elastic properties.

Model inputs include kerogen content, porosity, mineralogy (quartz, calcite, illite, chlorite, dolomite, and pyrite), pore-fluid saturations (bound water, free water, and free oil), pore aspect ratio, vitrinite reflectance, and kerogen type. The model outputs bulk modulus, shear modulus, and density, from which V_P and V_S are computed.

Elastic properties of clay minerals such as illite and chlorite show a wide range of reported values, largely due to variations in measurement techniques and the fine-grained, fluid-bound nature of clays (Mondol et al., 2008). Similarly, kerogen elastic properties remain poorly constrained (Vernik & Landis, 1996; Mavko et al., 2020). For this reason, the elastic properties of both kerogen and clay minerals (Illite and Chlorite) are treated as uncertain parameters in the rock physics model. These uncertain parameters were calibrated to the Theia-1 well using a Monte Carlo approach, as described in Huang et al. (2025a). The mineral properties used in the rock physics modeling are listed in Table 1.

TABLE 1

Table 1. Mineral properties used in rock physics modeling

Component	K [GPa]	μ [GPa]	ρ [g/cc]	Reference
Kerogen	9.2	3.6	$f(\%R_0)$	(Vernik and Landis, 1996; Mavko et al., 2020; Al Ibrahim et al., 2020)
Quartz	37	44	2.65	(Carmichael, 2017)
Calcite	76.8	32	2.71	(Simmons, 1965)

Illite	28.2	6.1	2.84	(Mondol et al., 2008; Wang et al., 2001)
Chlorite	39.2	8.8	2.71	(Mondol et al., 2008; Wang et al., 2001)
Dolomite	94.9	45	2.87	(Humbert, 1972)
Pyrite	139	112.3	5.01	(Whitaker et al., 2010)
Bound water	2.2	0	1.0	(Mavko et al., 2020)
Free water	2.2	0	1.0	(Mavko et al., 2020)
Oil	1.02	0	0.8	(Batzle & Wang, 1992)

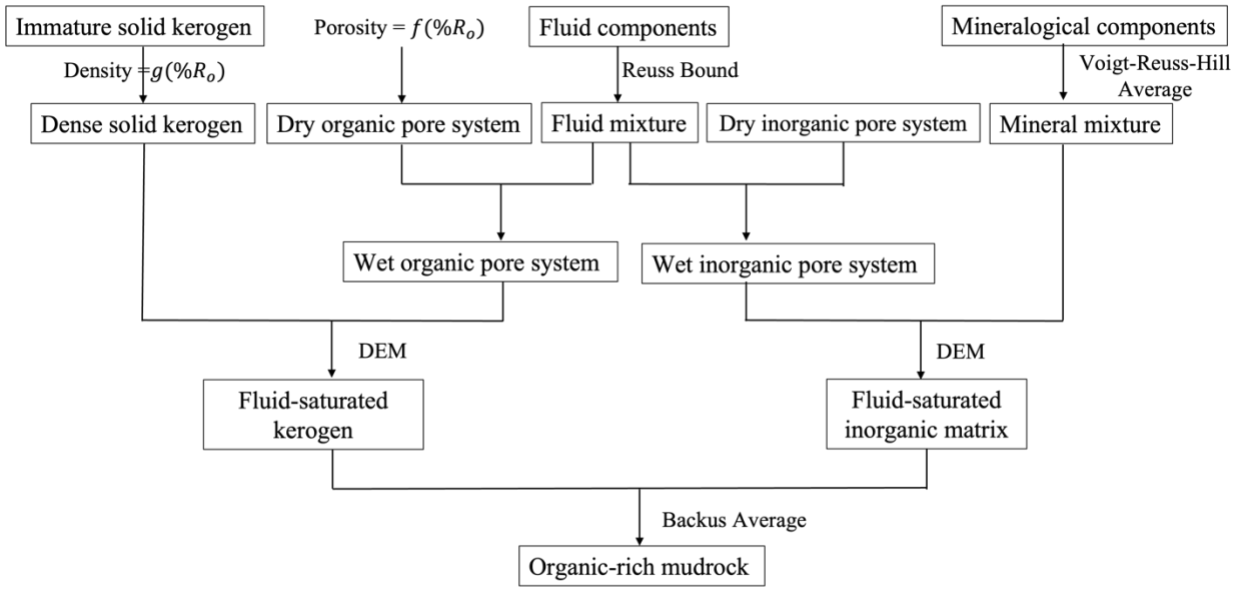

Figure 4. Thermal-maturation dependent rock physics model for organic-rich mudrocks (modified from Huang et al., 2025a).

Weighted ABC for rock physics inversion. The weighted ABC (Huang et al., 2025a) is applied to estimate the uncertain rock physics parameters in the rock physics model. ABC is suitable for this problem because the forward model is nonlinear, and a closed-form likelihood

function is not available. Prior distributions for porosity, kerogen, minerals, fluids, and other uncertain inputs are estimated from geological and laboratory knowledge (Table 2).

For each prior sample generated in the Monte Carlo sampling, the rock physics model generates synthetic (V_P, V_S, ρ). A weighted Mahalanobis distance is used to quantify the discrepancy between synthetic and observed (V_P, V_S, ρ) in the Theia-1 well, where weights reflect the relative importance and scale differences among the elastic properties. The weights are estimated based on the corresponding calibration errors. Samples with misfits below a predefined tolerance are accepted, and the corresponding input variables form the posterior distributions conditioned on the well data. The rock physics inversion is performed depth by depth in the well logs (Figure 5) and point by point in the seismic section. Further details of the weighted ABC implementation, including data normalization, weighted distance function calculation, sampling scheme, and acceptance criterion are described in Huang et al. (2025a).

TABLE 2

Table 2. Prior distributions of input variables used in the ABC inversion

Input variable	**Distribution**	**Range**
Kerogen type	Categorical	III (Iqbal et al., 2022)
Vitrinite reflectance	Uniform	(0.23, 1.6)
Kerogen	Uniform	(0, 0.15)
Porosity	Uniform	(0, 0.15)
Matrix aspect ratio	Uniform	(0.001, 0.2)
Quartz	Dirichlet	(0, 0.6)
Calcite	Dirichlet	(0, 0.8)

Illite	Dirichlet	(0, 0.8)
Chlorite	Dirichlet	(0, 0.1)
Dolomite	Dirichlet	(0, 0.1)
Pyrite	Dirichlet	(0, 0.06)
Bound water	Dirichlet	(0, 1)
Free water	Dirichlet	(0, 1)
Oil	Dirichlet	(0, 1)

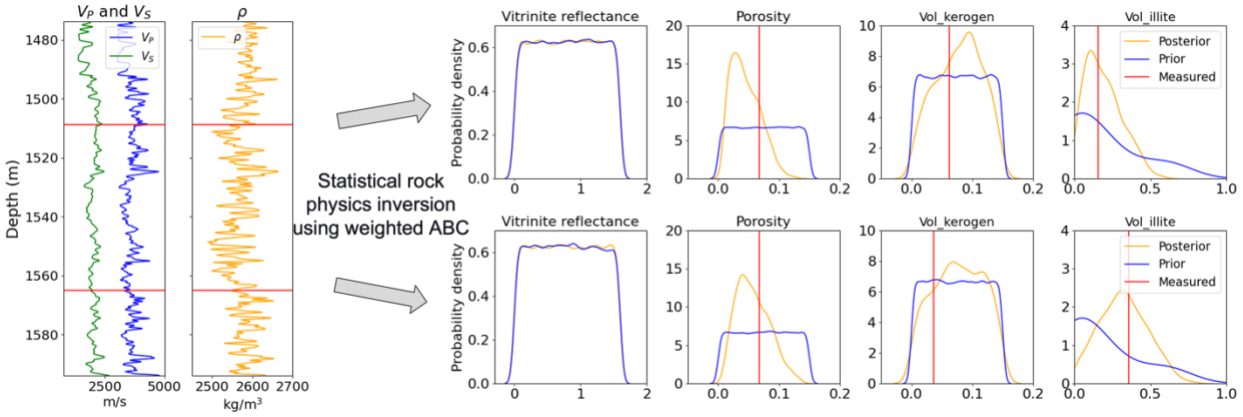

Figure 5. Schematic illustration of the weighted ABC rock physics inversion applied depth-by-depth to the Theia-1 well. The blue arrows indicate the inversion step, where synthetic (V_P, V_S, ρ) from the rock physics model are compared to the observed log values at the depths marked by the red horizontal lines. The subplots on the right show the prior (blue), posterior (orange), and measured (red) distributions of the elastic properties at those depths. Note that vitrinite reflectance shows no update from the prior to the posterior distribution.

Rock physics inversion results using seismic data. To improve the robustness of the inversion, seismic outliers are detected and removed using the robust Mahalanobis distance (RMD) (Rousseeuw, 1984), to ensures that noise, acquisition artifacts, and local geologic irregularities do not bias the posterior-based elastic property predictions. The weighted ABC inversion is then applied point-by-point to the 2D (V_P, V_S, ρ) sections to estimate the spatial distribution of source rock properties. The mean and interquartile range (IQR) of the inverted parameters are shown in Figure 6a and 6b, respectively. Porosity exhibits higher mean values in the deeper portion of the Goldwyer III unit, with relatively uniform IQR across the interval. Illite volume fraction shows higher mean values and increased variability near the top and bottom of the unit. Kerogen volume fraction is generally higher in the shallower to mid-depth interval, with modest uncertainty throughout. These results highlight lateral and vertical heterogeneity of source rock properties within the Goldwyer III unit.

A comparison between the inverted porosity, illite fraction, and kerogen fraction extracted at the Theia-1 well location and the corresponding logs (Figure 6c) shows that the inversion successfully reproduces the primary depth trends and magnitudes observed in the well data.

Although the rock physics inversion provides well-constrained estimates of porosity, kerogen content, and clay content, elastic properties are only weakly sensitive to thermal maturity, resulting in minimal posterior updating of vitrinite reflectance (Figure 5). In addition, key source-rock attributes such as transformation ratio and hydrocarbon generation are not directly constrained by the rock physics model. Therefore, inversion of elastic properties alone cannot fully resolve the thermal evolution or petroleum potential of the Goldwyer III source rock. To address this limitation, we integrate the inversion results with Monte Carlo basin modeling in the next section.

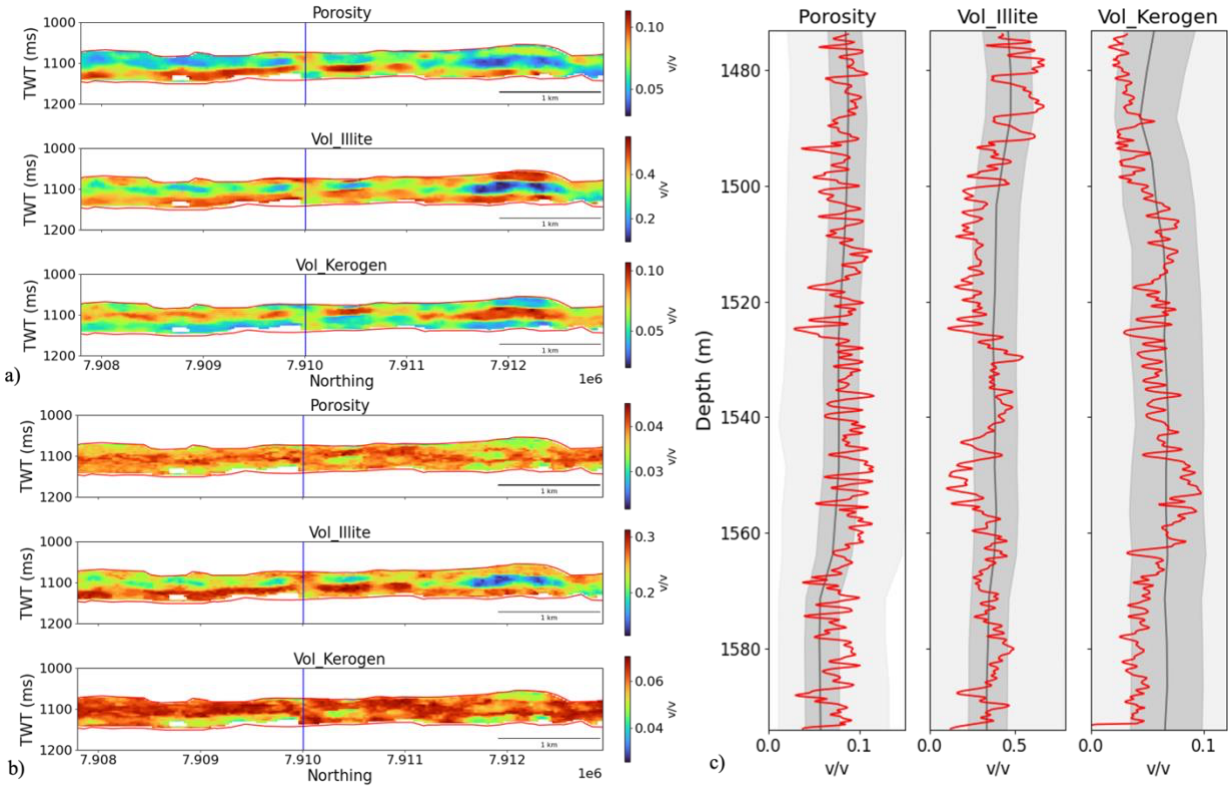

Figure 6. Spatial distributions of the posterior mean (a) and interquartile range (IQR) (b) for inverted porosity, illite volume fraction, and kerogen volume fraction within the Goldwyer III interval. The blue vertical line marks the location of the Theia-1 well. (c) Validation of inverted properties at the Theia-1 well, where the seismically-derived posterior estimates are compared with measured logs. Light gray shading represents the full range of accepted samples, dark gray represents the interquartile range, the dark gray line indicates the median, and red curves show the well-log measurements.

MONTE CARLO BASIN MODELING

Monte Carlo basin modeling extends the predictive capability of our workflow by incorporating geological history and kinetic processes that are not captured by elastic properties alone. Posterior distributions of petrophysical and compositional properties from the rock physics

inversion describe above are used as present-day constraints. Laboratory measurements, well logs, stratigraphic information, and tectonic evolution are integrated into the Monte Carlo framework to reconstruct the burial and thermal history of the Goldwyer III source rock and to probabilistically estimate its thermal maturity and hydrocarbon generation potential.

Monte Carlo simulations were conducted using the Stanford Basin and Petroleum System Modeling (BPSM) PetroMod Toolbox (Al Ibrahim, 2019), which automates multi-model construction, parameter sampling, simulation execution, and extraction of results for uncertainty analysis (Figure 7). Additional implementation details of the automated basin modeling workflow are described in Huang et al. (2025b).

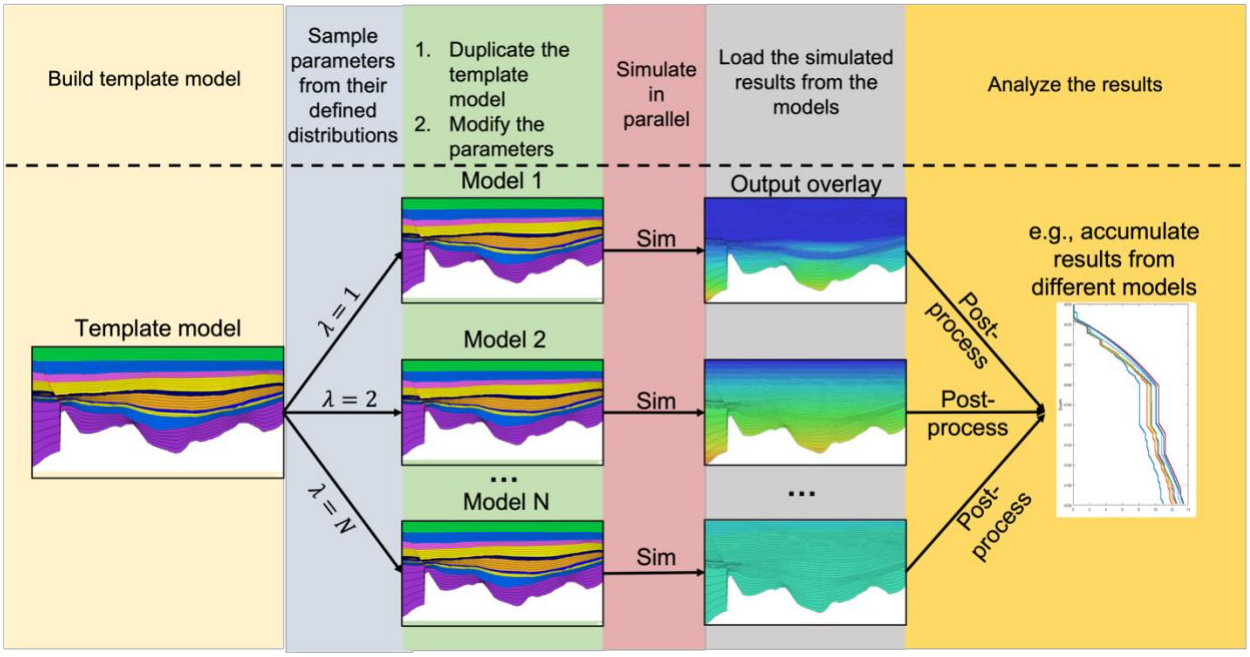

Figure 7. Workflow of the Monte Carlo basin modeling process. A template basin model is defined at the Theia-1 well, and uncertain geological and thermal parameters are sampled to generate multiple realizations. Each realization is simulated in parallel to reconstruct burial and thermal histories, and the results are aggregated to quantify uncertainty in source-rock maturity and hydrocarbon generation.

Basin modeling inputs and uncertainty specification. A 1D basin model template at the Theia-1 well provides the structural framework for the Monte Carlo simulations. Baseline geological, geochemical, and thermal inputs, including formation ages and thicknesses, erosion magnitudes, organic facies properties, and boundary conditions, are defined from well logs, geochemical measurements, inversion-derived elastic properties, and regional geological studies. These inputs establish a geologically consistent representation of the subsurface system.

Petrological inputs, including porosity, TOC, and mineral compositions, are derived from the posterior distributions obtained in Section 3 through statistical rock physics inversion. A 1D vertical column at the Theia-1 well is discretized into N layers within the Goldwyer III unit (N =17 in this study). For each layer, porosity, kerogen content, and mineral fractions (quartz, calcite, illite, chlorite, dolomite, and pyrite) are sampled from their respective posterior distributions. Porosity is used to estimate mechanical compaction via Athy's law (Athy, 1930), while kerogen volume fraction is converted to TOC assuming a kerogen-to-rock density ratio of approximately 1:2 (Al Ibrahim, 2019). Mineral fractions are sampled using Dirichlet distributions to ensure that the proportions sum to one (MacKay, 2003). This probabilistic formulation enables direct propagation of inversion-derived uncertainty into the basin modeling workflow (Figure 8).

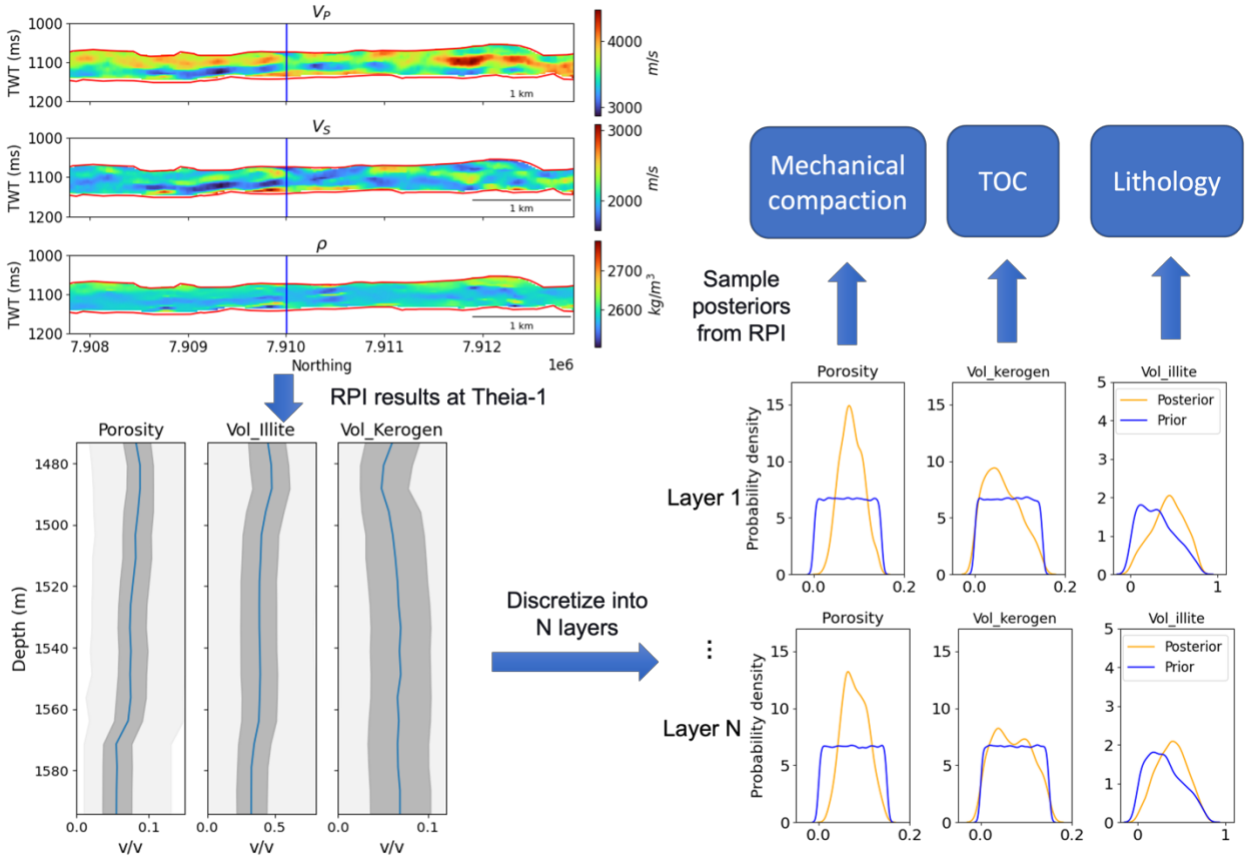

Figure 8. Schematic illustration of integrating rock physics inversion (RPI) with Monte Carlo basin modeling. Seismically-derived V_P, V_S, and ρ are inverted to obtain posterior distributions of source rock properties. The inverted properties at the well location are discretized into N layers for the basin modeling input table.

Paleo-erosion magnitude uncertainty for the Jurassic–Cretaceous and Carboniferous–Permian periods at Theia-1 is derived from regional erosion estimates reported by Johnson et al. (2017) and represented using truncated normal distributions (Virtanen et al., 2020) bounded by the published 95% confidence limits (Figure 9a).

Organic facies inputs are estimated using Rock-Eval pyrolysis data from the Theia-1 well (Johnson et al., 2020; Iqbal et al., 2022), where Hydrogen Index (HI) values range from 60 to 268

mg HC/g TOC. HI uncertainty is represented using a kernel density estimate (KDE), and kerogen within the Goldwyer III unit is classified mainly as Type II–III and Type III (Figure 9b; Peters & Cassa, 1994). For kinetics model, PetroMod default models for Type II–III and Type III kerogen (Pepper & Corvi, 1995) are sampled probabilistically with assignments guided by a discrete-time Markov chain (DTMC; Norris, 1998) to preserve vertical continuity in organic facies.

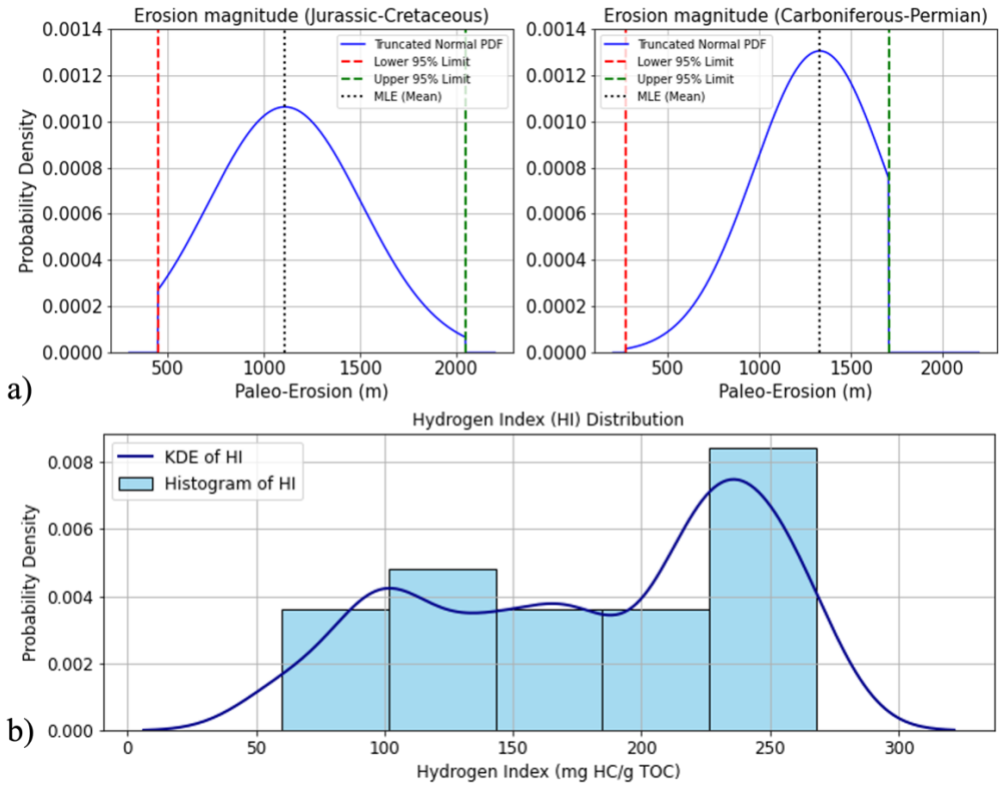

Figure 9. (a) Truncated normal distributions of paleo-erosion magnitudes during the Jurassic–Cretaceous and Carboniferous–Permian periods at the Theia-1 well. The mean values correspond to the maximum likelihood estimates, and the lower and upper bounds represent the 95% confidence limits derived from regional well constraints (Johnson et al., 2019; Virtanen et al., 2020). (b) Histogram and kernel density estimation (KDE) of Hydrogen Index (HI) from Rock-

Eval pyrolysis data, used to characterize the distribution of organic richness for the Monte Carlo basin modeling.

Geological boundary conditions and uncertainty specification. The basal thermal boundary condition is the paleo–heat flow (HF), which strongly influences hydrocarbon generation rates and timing in basin modeling (Hsu & Robinson, 2017). In this study, HF uncertainty is constrained using the regional tectonic history of the Canning Basin, with typical values for major tectonic phases adopted from Allen & Allen (2005). The resulting time-varying HF ranges are sampled using uniform distributions (Figure 10). Paleo-water depth (PWD) uncertainty is derived from depositional environment interpretations in the WAPIMS biostratigraphy database (Young et al., 2021; Tipsword et al., 1966) and similarly represented as uniform distributions through geological time (Figure 10). Seafloor water interface temperature (SWIT) is automatically calculated in PetroMod based on PWD and well location (Wygrala, 1989), and its temporal uncertainty is also shown in Figure 10. All boundary conditions are sampled only at geological time points where depositional and tectonic information are available, ensuring that the Monte Carlo realizations remain geologically consistent through time.

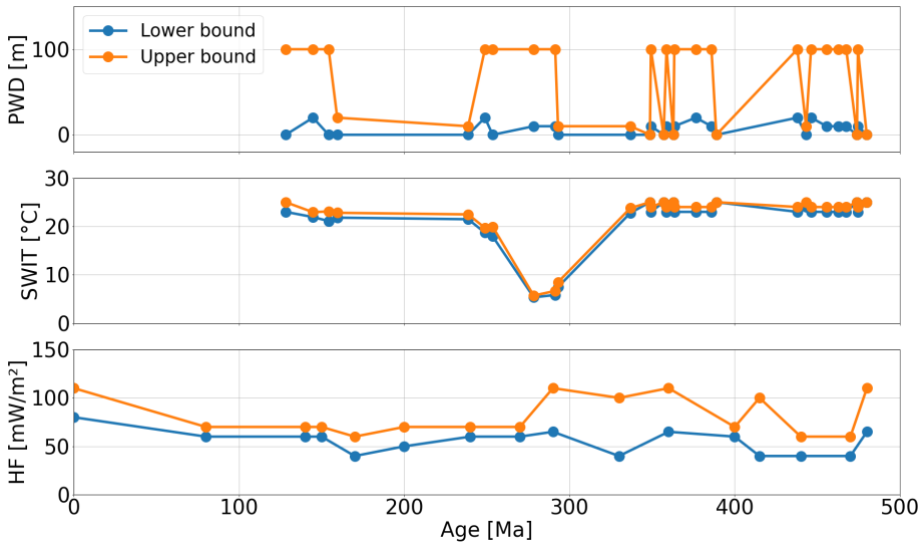

Figure 10. Estimated PWD, SWIT, and HF through geological time (Young et al., 2021; Finder exploration, 2018). The orange and blue curves represent upper and lower bounds respectively, and the corresponding dots represent estimated values constrained by depositional environment interpretations.

Simulation setup. A total of 500 Monte Carlo basin models were generated by duplicating the 1D template and updating only the input tables and boundary conditions described above, ensuring that all realizations share identical simulator settings. Several simulation parameters were adjusted from the defaults to improve numerical stability and temporal resolution: the maximum cell thickness was set to 5 m, consistent with the minimum layer thickness in the model, and the maximum time-step duration was limited to 0.25 Ma to better capture rapid burial and heating events. The number of geometric optimization iterations was set to 20 to ensure convergence of forward stratigraphic reconstruction while maintaining computational efficiency. Core measurements indicate extremely low matrix permeability and porosity (<10%) in the Goldwyer III unit (Finder Exploration, 2018), suggesting limited matrix-scale expulsion (Jarvie, 2012;

Sondergeld et al., 2010). Therefore, a low expulsion efficiency scenario was adopted using a 10% expulsion factor, while enabling organic secondary porosity, secondary cracking, and radiogenic heat generation to account for shale-specific retention and maturation processes.

Monte Carlo basin modeling results. Depth-dependent distributions of vitrinite reflectance, transformation ratio (TR), temperature, and pore pressure are shown in Figure 11. Variability among realizations reflects the combined uncertainty in petrophysical properties, organic facies, erosion magnitudes, and thermal boundary conditions sampled in the Monte Carlo simulations. Key observations are summarized below:

• **Vitrinite reflectance ($\%R_o$)**: $\%R_o$ increases with depth across all realizations. Within the Goldwyer III unit, values range from 0.7 to 1.5 $\%R_o$, with an interquartile range of 0.8 to 1.1 $\%R_o$. These estimates place the interval within the oil to wet-gas windows (Kibria et al., 2020). Uncertainty increases at depth, reflecting sensitivity to erosion and paleo-heat-flow history, which strongly influence accumulated thermal stress.

• **Transformation ratio (TR)**: TR also increases with depth and shows substantial variability, ranging from 10% to 90% across realizations, with a median of 70% and interquartile range of 50–80%. This indicates widespread but not fully exhausted hydrocarbon generation potential.

• **Temperature**: Temperature uncertainty gradually broadens with depth but remains narrower than maturity-related outputs. Median temperatures at the top and base of Goldwyer III are approximately 95 °C and 100 °C, respectively. The measured bottom-hole temperature falls within the interquartile range, supporting consistency between modeled and observed thermal conditions.

• **Pore pressure**: Pore pressure predictions exhibit comparatively low spread. Above Goldwyer III, most realizations remain near hydrostatic conditions. Within the unit, modest overpressure variability occurs but remains limited, largely because pressure simulation is tied to porosity-controlled compaction and permeability, which are only uncertain within Goldwyer III in our Monte Carlo setup.

Overall, vitrinite reflectance and TR show the greatest sensitivity to uncertain inputs, while temperature and pore pressure remain more tightly constrained.

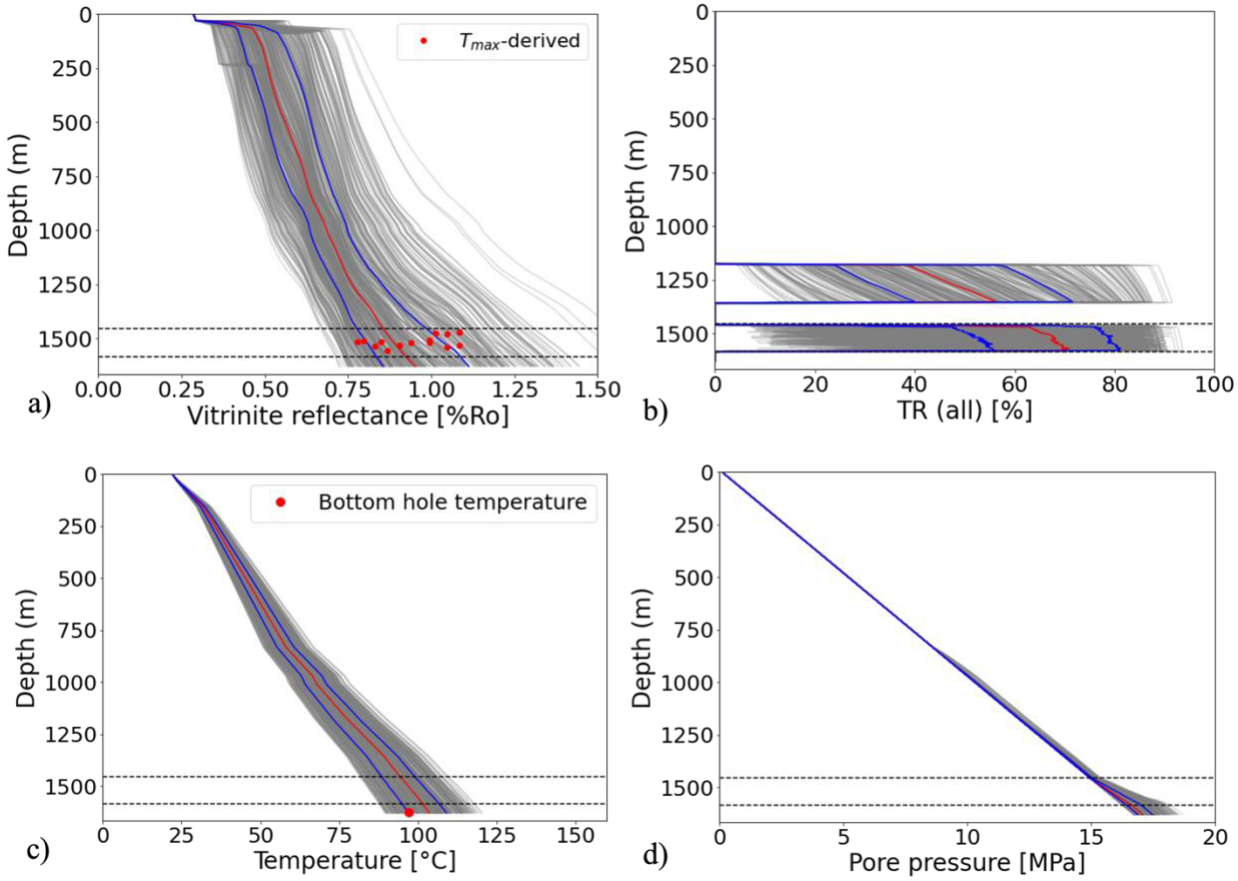

Figure 11. Monte Carlo simulation results for vitrinite reflectance (thermal maturity), transformation ratio (TR), temperature, and pore pressure. The light grey lines show individual basin model realizations, blue lines denote the 25th and 75th percentiles, and red lines represent

the median estimates. The black dash lines mark the top and base of the Goldwyer III interval. Red dots in the vitrinite reflectance panel are calculated using a T_{max}-based empirical correlation (Jarvie, 2001), and the red dot in the temperature panel indicates the measured bottom-hole temperature.

THERMAL MATURITY UNCERTAINTY REDUCTION THROUGH THE INTERGRATED WORKFLOW

A major benefit of incorporating Monte Carlo basin modeling into the workflow is the improved constraint on thermal maturity, which is difficult to resolve using present-day elastic properties alone. To demonstrate this impact, we compare vitrinite reflectance predictions from three approaches: (1) the integrated workflow developed in this study, where statistical rock physics inversion provides present-day constraints that are propagated through Monte Carlo basin modeling; (2) vitrinite reflectance inferred directly from rock physics inversion, which reflects only current elastic signatures (Huang et al., 2025a); and (3) T_{max}-based empirical estimates derived from geochemical measurements (Jarvie, 2001).

Figure 12 shows that the T_{max}-derived vitrinite reflectance values lie almost entirely within the range of Monte Carlo predictions and generally fall inside the interquartile envelope, indicating strong consistency with the integrated results. In contrast, the posterior distribution from rock physics inversion alone remains broad and shows minimal narrowing relative to its prior, confirming that present-day elastic properties provide limited sensitivity to maturity. By incorporating basin geohistory, kinetic processes, and boundary-condition uncertainty, the integrated workflow significantly reduces uncertainty in thermal maturity estimates while maintaining consistency with available observations.

These results highlight that Monte Carlo basin modeling provides critical additional constraints on maturity beyond what can be inferred from seismic and well-log signatures, enhancing confidence in source-rock evaluation and reducing exploration risk.

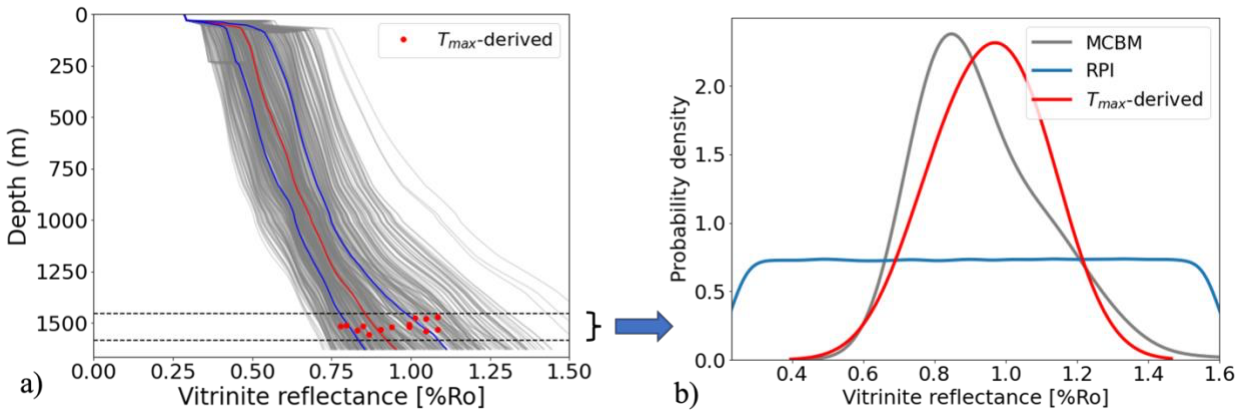

Figure 12. Comparison of vitrinite reflectance estimates from multiple sources. (a) Monte Carlo basin modeling results compared with T_{max}-derived vitrinite reflectance. The grey lines represent individual basin model realizations, blue lines denote the 25th and 75th percentiles, and the red line indicates the median. The black dash lines mark the top and base of the Goldwyer III interval. Red dots represent vitrinite reflectance values calculated from Tmax (Jarvie, 2001). (b) Vitrinite reflectance distributions within the Goldwyer III interval derived from Monte Carlo basin modeling (grey), the rock physics inversion posterior (blue), and T_{max}-based estimates (red).

CONCLUSION

This study demonstrates that statistical rock physics inversion and Monte Carlo basin modeling provide complementary constraints for source rock evaluation when integrated into a unified workflow. Elastic data effectively constrain composition-controlled properties such as porosity, kerogen content, and mineral fractions, while basin modeling leverages geological

history and kinetic processes to resolve thermally controlled properties such as thermal maturity and transformation ratio. This division of sensitivity enables each method to compensate for the other's intrinsic limitations, yielding a more complete and reliable characterization of source rock systems than either approach alone.

Despite these strengths, some limitations remain. The modeling relies on parameterizations of heat flow, erosion, and kerogen kinetics that carry their own uncertainties, particularly in regions with sparse calibration data. Furthermore, while a 1D model captures local vertical trends effectively, lateral variations in structure, hydrodynamics, or fracture-controlled expulsion may not be fully represented. These exceptions suggest opportunities for extending the workflow to 2D or 3D domains and to datasets with more comprehensive calibration.

Overall, this work establishes a generalizable and practical approach for quantitative source rock assessment with explicit uncertainty tracking. By integrating statistical inversion of seismic and well-log data with physics-based basin modeling, the workflow reduces the uncertainty in evaluation of hydrocarbon generation potential and improves confidence in exploration decisions, particularly in frontier or data-limited settings. This framework forms a foundation for future advances that couple geological, geophysical, geochemical, and geomechanical processes into a unified predictive system for subsurface resource characterization.

ACKNOWLEDGEMENTS

This work was supported by funding from the sponsors of the Stanford Center for Earth Resources Forecasting (SCERF) and the Stanford Natural Gas Initiative (NGI). We thank Western Australia's Department of Mines, Industry Regulation and Safety and Partha Pratim Mandal for

providing key data used in this study. We also acknowledge Lukman Mobolaji Johnson for helpful discussions.

DATA AND MATERIALS AVAILABILITY

Data associated with this research are available and can be obtained by contacting the corresponding author.

REFERENCE

Al Ibrahim, M., 2019, Petroleum system modeling of heterogeneous organic-rich mudrocks: Ph.D. thesis, Stanford University.

Al Ibrahim, M. A., T. Mukerji, and A. Hosford Scheirer, 2020, A thermal-maturation dependent elastic rock physics template for organic-rich mudrocks: Construction and application: Fifth EAGE Workshop on Rock Physics, European Association of Geoscientists & Engineers, Expanded Abstracts, 1–5, https://doi.org/10.3997/2214-4609.2020603028.

Alfred, D., and L. Vernik, 2012, A new petrophysical model for organic shales: SPWLA Annual Logging Symposium, Society of Petrophysicists and Well Log Analysts.

Allen, P. A., and J. R. Allen, 2005, Basin analysis: Principles and applications: Blackwell Publishing, 2nd ed.

Athy, L. F., 1930, Density, porosity, and compaction of sedimentary rocks: AAPG Bulletin, **14**, 1–24.

Avseth, P., T. Mukerji, G. Mavko, and J. Dvorkin, 2010, Rock-physics diagnostics of depositional texture, diagenetic alterations, and reservoir heterogeneity in high-porosity siliciclastic sediments and rocks—A review of selected models and suggested work flows: GEOPHYSICS, **75**, no. 5, 75A31–75A47.

Backus, G. E., 1962, Long-wave elastic anisotropy produced by horizontal layering: Journal of Geophysical Research, **67**, 4427–4440.

Batzle, M., and Z. Wang, 1992, Seismic properties of pore fluids: GEOPHYSICS, **57**, 1396–1408.

Berryman, J. G., 1995, Mixture theories for rock properties, in Rock physics and phase relations: A handbook of physical constants, T. J. Ahrens, ed.: American Geophysical Union, 205–228.

Bosch, M., T. Mukerji, and E. F. Gonzalez, 2010, Seismic inversion for reservoir properties combining statistical rock physics and geostatistics: A review: GEOPHYSICS, **75**, no. 5, 75A165–75A176.

Carmichael, R. S., 2017, Practical handbook of physical properties of rocks and minerals: CRC Press.

D'Ercole, C., L. Gibbons, and K. A. R. Ghori, 2003, Prospects and leads, central Canning Basin, Western Australia, 2003 (Record 2003/14): Western Australia Geological Survey.

Finder Exploration, 2018, Maturity and unconventional resource modelling: April 2018 update for Finder Exploration's Pan-Canning Goldwyer unconventional limit project (PC-GULP): PowerPoint slides, Finder Exploration, https://wapims.dmp.wa.gov.au/WAPIMS/

Fonseca, J., A. Pradhan, and T. Mukerji, 2023, Bayesian geophysical basin modeling with seismic kinematic metrics to quantify uncertainty for pore pressure prediction: GEOPHYSICS, **88**, no. 6, M239–M259.

Foster, C. B., G. W. O'Brien, and S. T. Watson, 1986, Hydrocarbon source potential of the Goldwyer Formation, Barbwire terrace, Canning basin, Western Australia: APPEA Journal, **26**, 142–155.

Galford, J., J. Quirein, D. Westacott, and J. Witkowsky, 2013, Quantifying organic porosity from logs: SPWLA Annual Logging Symposium, Society of Petrophysicists and Well Log Analysts.

Ghori, K. A. R., and P. W. Haines, 2007, Paleozoic petroleum systems of the Canning Basin, Western Australia: A review: Search and Discovery, **5**.

Grana, D., L. Azevedo, L. De Figueiredo, P. Connolly, and T. Mukerji, 2022, Probabilistic inversion of seismic data for reservoir petrophysical characterization: Review and examples: GEOPHYSICS, **87**, no. 5, M199–M216.

Haines, P. W., 2011, Geology, exploration history, and petroleum prospectivity of state acreage release area L11-5, Canning Basin, Western Australia: Geological Survey of Western Australia, 1–10.

Hansen, J. A., N. H. Mondol, and M. Fawad, 2019, Organic content and maturation effects on elastic properties of source rock shales in the Central North Sea: Interpretation, **7**, T477–T497.

Hantschel, T., and A. I. Kauerauf, 2009, Fundamentals of basin and petroleum systems modeling: Springer Science & Business Media.

Huang, J., A. H. Scheirer, and T. Mukerji, 2025, Statistical rock physics inversion for assessing source rock properties from seismic signatures: An application to the Canning Basin, Australia: Journal of Applied Geophysics, article 106026.

Huang, J., and T. Mukerji, 2025, Assessing uncertainty of source rock properties using Monte Carlo basin modeling–Application to Canning Basin, Australia: EarthArXiv, https://doi.org/10.31223/X5DN0P

Humbert, P., 1972, Propriétés élastiques de carbonates rhombohédriques monocristallins: Calcite, magnésite, dolomite: Comptes Rendus de l'Académie des Sciences Paris, **275**, 391.

Hsu, C. S., and P. R. Robinson, eds., 2017, Springer handbook of petroleum technology: Springer.

Iqbal, M. A., R. Rezaee, C. Laukamp, B. Pejcic, and G. Smith, 2022, Integrated sedimentary and high-resolution mineralogical characterisation of Ordovician shale from Canning Basin, Western Australia: Implications for facies heterogeneity evaluation: Journal of Petroleum Science and Engineering, **208**, article 109347.

Jarvie, D. M., B. L. Claxton, F. Henk, and J. T. Breyer, 2001, Oil and shale gas from the Barnett Shale, Fort Worth basin, Texas: AAPG annual meeting program, **10**, A100.

Jarvie, D. M., 2012, Shale resource systems for oil and gas: Part 2 — Shale-oil resource systems, in J. A. Breyer, ed., Shale reservoirs — Giant resources for the 21st century: AAPG Memoir **97**, 89–119.

Johnson, L. M., R. Rezaee, A. Kadkhodaie, G. Smith, and H. Yu, 2017, A new approach for estimating the amount of eroded sediments, a case study from the Canning Basin, Western Australia: Journal of Petroleum Science and Engineering, **156**, 19–28.

Johnson, L. M., R. Rezaee, G. C. Smith, N. Mahlstedt, D. S. Edwards, A. Kadkhodaie, and H. Yu, 2020, Kinetics of hydrocarbon generation from the marine Ordovician Goldwyer Formation, Canning Basin, Western Australia: International Journal of Coal Geology, **232**, article 103623.

Kibria, M. G., S. Das, Q. H. Hu, A. R. Basu, W. X. Hu, and S. Mandal, 2020, Thermal maturity evaluation using Raman spectroscopy for oil shale samples of USA: Comparisons with vitrinite reflectance and pyrolysis methods: Petroleum Science, **17**, 567–581.

Li, Y., Z. Q. Guo, C. Liu, X. Y. Li, and G. Wang, 2015, A rock physics model for the characterization of organic-rich shale from elastic properties: Petroleum Science, **12**, 264–272.

MacKay, D. J., 2003, Information theory, inference and learning algorithms: Cambridge University Press.

Mavko, G., T. Mukerji, and J. Dvorkin, 2020, The rock physics handbook: Cambridge University Press.

Mondol, N. H., J. Jahren, K. Bjørlykke, and I. Brevik, 2008, Elastic properties of clay minerals: The Leading Edge, **27**, 758–770.

Norris, J. R., 1998, Markov chains: Cambridge University Press.

Rousseeuw, P. J., 1984, Least median of squares regression: Journal of the American Statistical Association, **79**, 871–880.

Rubin, D. B., 1984, Bayesianly justifiable and relevant frequency calculations for the applied statistician: Annals of Statistics, **12**, 1151–1172.

Pacchiardi, L., P. Künzli, M. Schöngens, B. Chopard, and R. Dutta, 2021, Distance-learning for approximate Bayesian computation to model a volcanic eruption: Sankhya B, **83**, 288–317.

Peters, K. E., and M. R. Cassa, 1994, Applied source rock geochemistry.

Pepper, A. S., and P. J. Corvi, 1995, Simple kinetic models of petroleum formation: Part I: Oil and gas generation from kerogen: Marine and Petroleum Geology, **12**, 291–319.

Peters, K. E., O. Schenk, A. Hosford Scheirer, B. Wygrala, and T. Hantschel, 2017, Basin and petroleum system modeling: Springer International Publishing, 381–417.

Pradhan, A., and T. Mukerji, 2020, Seismic Bayesian evidential learning: Estimation and uncertainty quantification of sub-resolution reservoir properties: Computational Geosciences, **24**, 1121–1140.

Simmons, G., 1965, Single crystal elastic constants and calculated aggregate properties: Journal of the Graduate Research Center, **34**, 1.

Sondergeld, C. H., K. E. Newsham, J. T. Comisky, M. C. Rice, and C. S. Rai, 2010, Petrophysical considerations in evaluating and producing shale gas resources: SPE Unconventional Resources Conference/Gas Technology Symposium, Society of Petroleum Engineers, SPE-131768.

Sweeney, J. J., and A. K. Burnham, 1990, Evaluation of a simple model of vitrinite reflectance based on chemical kinetics: AAPG Bulletin, **74**, 1559–1570.

Tipsword, H. L., F. M. Setzer, and F. L. Smith Jr., 1966, Interpretation of depositional environment in Gulf Coast petroleum exploration from paleoecology and related stratigraphy: Gulf Coast Association of Geological Societies Transactions, **16**, 119–130.

Tong, Y., and T. Mukerji, 2017, Generalized sensitivity analysis study in basin and petroleum system modeling, case study on Piceance Basin, Colorado: Journal of Petroleum Science and Engineering, **149**, 772–781.

Vernik, L., and C. Landis, 1996, Elastic anisotropy of source rocks: Implications for hydrocarbon generation and primary migration: AAPG Bulletin, **80**, 531–544.

Virtanen, P., R. Gommers, T. E. Oliphant, M. Haberland, T. Reddy, D. Cournapeau, and P. Van Mulbregt, 2020, SciPy 1.0: Fundamental algorithms for scientific computing in Python: Nature Methods, **17**, 261–272.

Wang, Z., H. Wang, and M. E. Cates, 2001, Effective elastic properties of solid clays: GEOPHYSICS, **66**, 428–440.

Whitaker, M. L., W. Liu, L. Wang, and B. Li, 2010, Acoustic velocities and elastic properties of pyrite (FeS_2) to 9.6 GPa: Journal of Earth Science, **21**, 792–800.

Wygrala, B. P., 1989, Integrated study of an oil field in the southern Po Basin, northern Italy: Ph.D. thesis, Kernforschungsanlage Juelich GmbH and University of Cologne.

Young, A., N. Flament, L. Hall, and A. Merdith, 2021, The influence of mantle flow on intracontinental basins: Three examples from Australia: Basin Research, **33**, 1429–1453.